Image-Guided Surgical and Pharmacotherapeutic Routines as Part of Diligent Medical Treatment

Adel Razek

applied sciences

MDPI

Review

Image-Guided Surgical and Pharmacotherapeutic Routines as Part of Diligent Medical Treatment

Adel Razek

Group of Electrical Engineering—Paris (GeePs), CNRS, University of Paris-Saclay and Sorbonne University, F91190 Gif sur Yvette, France; adel.razek@centralesupelec.fr

Abstract: This contribution is part of the objective of diligent universal care that ensures the well-being of a patient. It aims to analyze and propose enriched image-guided procedures for surgical interventions and restricted delivery of implanted drugs in minimally invasive and non-ionizing circumstances. This analysis is supported by a literature review conducted in two ways. The first aims to illustrate the importance of recent research and applications involved in different topics of the subject; this is mainly the case for the introduction's literature. The second concerns the literature dedicated to having more detailed information in context; this mainly concerns the citations in the different sections of the article. The universal goals of medical treatments are intended to involve the well-being of the patient and allow medical personnel to test new therapies and carry out therapeutic training without risk to the patient. First, the various functionalities involved in these procedures and the concerns of the magnetic resonance imaging technique (MRI) and ultrasound imaging technique (USI), recent contributions to the subject are reviewed. Second, the intervention procedures guided by the image and the implemented actions are analyzed. Third, the components of the fields involved in MRI are examined. Fourth, the MRI control of the treatments, its performance and its compliance are analyzed. Compatibility with MRI via electromagnetic compatibility (EMC) is conferred and demonstrated for an actuation example. Fifth, the extension of the concepts mentioned in the article, in the context of patient comfort and the training of medical staff is proposed. The main contribution of this article is the identification of the different strategic aids needed in healthcare related to image-assisted robotics, non-ionized, minimally invasive and locally restrictive means. Furthermore, it highlights the benefits of using phantoms based on real biological properties of the body, digital twins under human control, artificial intelligence tools and augmented reality-assisted robotics.

Keywords: MRI-control; surgical interventions; implanted drug delivery; image-guided robotics; compliant treatment; MRI-compatibility

Citation: Razek, A. Image-Guided Surgical and Pharmacotherapeutic Routines as Part of Diligent Medical Treatment. *Appl. Sci.* **2023**, *13*, 13039. https://doi.org/10.3390/app132413039

Academic Editors: Vladislav Toronov and Jianbo Gao

Received: 25 September 2023
Revised: 29 November 2023
Accepted: 4 December 2023
Published: 6 December 2023

1. Introduction

Over the past few decades, medical procedures have moved from a direct fully invasive "hand-eye" pairing process to a minimal invasive (MI) process with robot-imaging pairing in a closed-loop treatment architecture. Acts related to the invasive nature mainly concern surgical interventions (Sis) and the restricted dispensing of drugs. Currently, both of these procedures can use MI image-guided (IG) robotics, which enables patient comfort and safety, and medical staff accuracy and efficiency. MI surgeries can be performed on most parts of the body, and the restricted drug delivery (RDD) that can be accomplished by implanted therapies, helps prevent the generalization of drugs throughout the body. Most imaging devices can be used in IG procedures. However, different imaging techniques are each tolerable for a specific situation. For example, those involving ionizing radiation would not be suitable for long interval exposure actions. In such a case, only the two imaging techniques exerting non-ionizing (NI) characteristics can be used; namely magnetic resonance imaging technique (MRI) and ultrasound imaging technique (USI).

An Imaging device is supposed to provide high-resolution 3D picturing of target configuration and neighboring material, including treatment instruments. Robotic assistance works normally within the imaging scaffold along with the target throughout imaging, permitting cooperative tasks to monitor treatment in a closed-loop mode. This can include pursuing target motion and deformation, localizing robotized equipment, and supervising therapy release. With the ever-increasing medical use of imaging technique-robot linked procedures, this presaged a new methodology to aid treatment techniques that allow medical staff to supervise patients better and more efficiently. Positioning robotic organizations within the frame of the scanner allows for a synergy of the imaging's visual ability and the robotic assistant's manipulation skill, resulting in closed-loop processing. With respect to imaging techniques with non-ionizing behavior, both MRI and USI reflect the characteristics mentioned above regarding imaging devices. Note that both imaging techniques can work in procedures with MI, IG, and NI for either SI or RDD operations. It should be noted that the only difference in behavior between these two imaging techniques is that the USI can only operate in airless and boneless windows. Additionally, operational precautions are required for MRI, for which the scaffolding environment must be free of electromagnetic (EM) noise. Nevertheless, MRI seems to be the universal imaging tool conditional to avoiding EM noise.

Robotic systems mainly contain actuation and sensing components. In the case of MRIs, the whole system is made of non-magnetic and non-conductive materials. This assumes that actuators and sensors contain negligible magnetic and conductive materials. Given that the scanner, is hyper sensitive to electromagnetic disturbances, questions on MRI-IG robots' presence in this environment are of concern. Matters that do not disturb the scanner are called MRI-compatible and those that are disruptive are labelled MRI-incompatible. The latter produce artifacts deteriorating the images. The scanner compatibility relates to its functional ability and can be controlled via functional control (FC) analysis. For MRI, FC analysis is via electromagnetic compatibility (EMC) analysis.

Although SI and RDD robotic actions can behave autonomously, medical staff can supervise and modify their conducts via remote control of the procedure. In other words, the robot-imaging duo that replaced the hand-eye one is still mastered in a different way.

The different issues related to IG treatments in MI and NI circumstances are widely covered in the literature, and in particular in recent research and applications in several medical fields. We have selected a few samples of each item representing different treatments. In the next paragraphs, this recent literature will be presented to show the wealth of current activity on the subject.

Regarding SI, many contributions have been proposed recently, see examples [1–7]. These selected examples of recent works show different interests of SI using MRI or USI. Two of them are reviews of state of the art MRI-guided robotic interventions. The other five concern different applications, myocardial perfusion without exogenous contrast agents, artificial intelligence-assisted ultrasound-guided robotic trans-carotid revascularization, MRI safety considerations for MRI-guided radiotherapy, intraoperative transapical cardiac MRI-guided intervention and MR conditional biopsy, and ablation needle tip artifacts. For research concerning imaging performance in general, see examples [8–13]. These include different imaging of metastatic spinal cord compression, pediatric body imaging, MRI cephalometric, and muscle fatty infiltration. Artifacts in images due to incompatibility of external insertions were also investigated, see examples [14–20]. These concern artifacts mainly in MRI due to metals, MRI artifact, and evaluation of pre examination screening, effects of metallic biomaterial, metal-artifact reduction, imaging-phantom study, imaging for periprosthetic joint infection, off-resonance artifact correction, and metal artifacts from passive implants. Several studies on safety conditions related to imaging techniques are reported, e.g., [21–24]. These concern safety in radiation therapy, radiofrequency-induced implant heating, active auditory implants, and metallic implants. New or improved designs of scanners are given in examples [25–31]. These improvements concern breast intervention robot, reducing MRI susceptibility artefacts in implants, hip arthroplasty implants with

metal artifact correction, improving MR image quality in metallic implants, superconducting magnet designs and MRI accessibility, improved visualization in patients with implants, and 3D-printing techniques for optimized imaging compatibility. Numerous investigations have been carried out on MRI-compatible devices; see examples [32–41]. These concern MRI-compatible devices in cardiac MRI, compatible fiber optic multi sensor, self-supervised reconstruction of gradient descent, safe robotic manipulator, compatible robots, compatible endonasal surgical robotic system, imaging-enhanced cranial neurosurgery, plastic piezoelectric motor stator, and compatible piezoelectric motors.

Recent work considering RDD has been reported in the literature; see e.g., [42–50]. These regard USI-guided DD enhancement, microbubble-mediated USI DD, microneedle patches for DD, DD to cancer cells, spatial, temporal, and dose control of DD, nanoparticles-based strategies to improve the delivery of therapeutic RNA in precision oncology, nanoparticle-based delivery systems in pancreatic cancer, and nano-drug delivery system for cancer. Contributions on implanted technologies and their concerns could be found, e.g., in [51–59]. These concern artefacts of biodegradable magnesium-based implants, assessment of implant-related pain and dysfunction, cochlear implant positioning and MR imaging quality, adverse local tissue reactions near metal implants after total hip arthroplasty, metal artefact reduction sequences for a piezoelectric bone conduction implant, image quality and artifact reduction of a cochlear implant, MRI in patients with cardiac implantable electronic devices, and MRI artifacts caused by auditory implants. Implanted treatment structures might manage confined conduct MI-imbedded equipment. These structures employ RDD for nearby tissue containing a specified area. Implanted treatments designate at best the practice of biodegradable ingredients and at least materials compatible with the treatment [60–71], as well as wireless operated implanted actuations.

The evolution, described in the above lines, from early hand-eye pairing of SI and RDD until robot-imaging IG controlled MI- and NI-universal procedure using MRI under FC (EMC analysis) and hand-eye supervision is schematically summarized (Memento) in Figure 1.

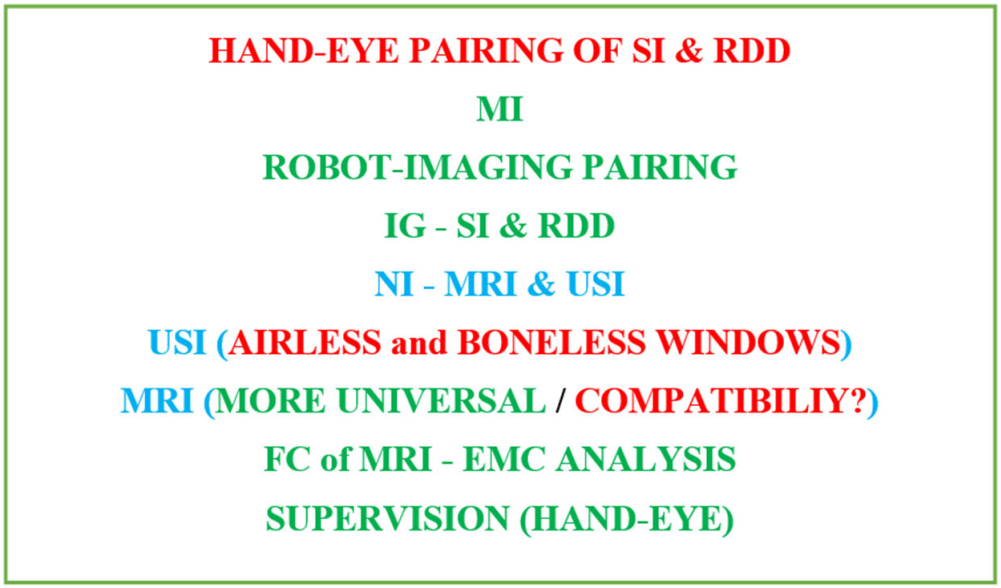

Figure 1. Summarized (Memento) successive evolution of surgical and pharmacotherapeutic routines following diligent medical treatment.

This contribution aims to review, analyze, and confer MI and NI procedures of SI and implanted RDD using IG robotics.

The second section of the paper assesses and analyzes image guided medical procedures involving surgical interventions and implantable drug delivery schemes as well

as their functional required specifications. The third section describes and illustrates the different field components of MRI and discusses safety issues related to these components. In the fourth section, the MRI-controlled treatments performance and compliance are analyzed and exhibited. This involves a compatibility compliance check of electromagnetic field perturbations and EMC conformity control applied to an actuation example. The fifth section offers a discussion of possible extensions of the different paper concepts from the perspective of patient well-being, staff training, and task verification.

2. Image Guided Medical Procedures

As mentioned earlier, mildly intrusive automated surgical or therapeutic treatments have emerged as an important tool in current medication. This involves IG robotics of SI and implanted therapies. It characterizes the advantages of MI treatment, e.g., faster catch-up intervals for patients, and escapes many of its disadvantages for medical personnel, e.g., disturbed pointer-vision matching and lack of autonomy within the treatment of the concerned body portion of the patient. Thus, the automated MI treatment reduces the body and mental burden after the staff weigh it. Nevertheless, offering personalized and appropriate support to further improve clinical performance remains a subject of exploration. Figure 2 illustrates schematics principle of IG medical procedures, involving medical environment (surgery, implanted therapeutic, etc.), medical tools (surgical needle, drug source, etc.), and medical data (action, position, etc.).

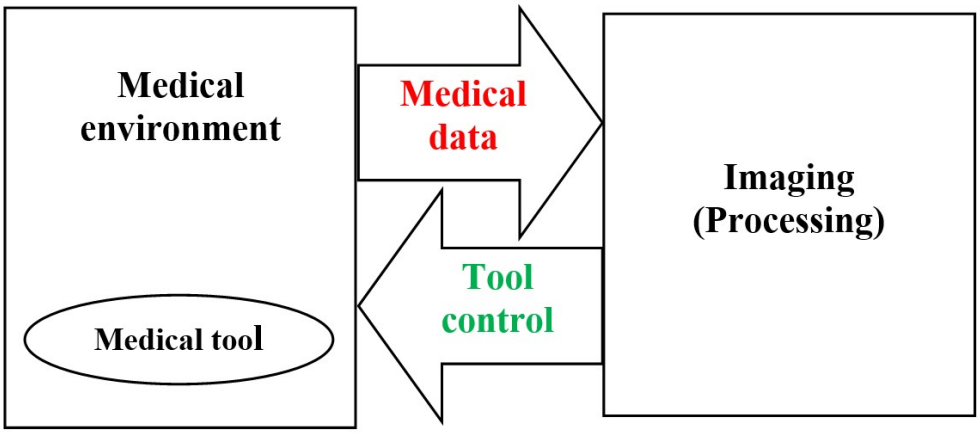

Figure 2. Schematics principle of IG medical treatment.

As mentioned earlier, choosing NI behavior involves using IRM or USI for IG operation of SI or RDD. As discussed and summarized in Figure 1, MRI appears to be suitable for all parts of the body without restriction. Due to its universal character, we will focus on MRI analysis, knowing that the USI can be used if it is suitable for the materials examined. Note that USI reflects good maneuverability and reasonable cost while MRI, despite producing soft tissue imaging, is more complicated and expensive. Therefore, from the point of view of practical use, the choice between the two imaging techniques depends on the situation. Therefore, the USI must be used whenever possible, even for interventions. Only in cases involving bone and/or air, such as the brain and many other parts of the body, should we use MRI. Normally, surgical centers performing MRI-assisted treatments are expected to have surgical-imaging rooms and do not need to move the scanner. Regarding imaging costs, if the well-being of the patient is taken into account, the only option for non-ionizing and minimally invasive treatment regarding a brain intervention, for example, is an MRI-assisted intervention.

Indeed, MRI can deliver high-grade 3D imagining of object structure, nearby tissue, and instruments; however, there are substantial challenges in its use for effectually guiding SI or RDD procedures. These challenges consist of the use of three magnetic fields of dissimilar natures (as we will see later), allergic reactions to EM noise, and the restrained

work area inside the imaging scaffold. This last drawback can be overcome by using an open structure scanner while accepting the disadvantage of a lower field intensity and therefore slower operation. On the other hand, MRI appears to be superior to other imaging strategies for different reasons. In addition to its NI behavior, it exhibits exceptional contrast allowing the visualization of tumors as well as other characters not detectable by other imaging techniques. It has true 3D-imaging potential, including multimodal detection, e.g., blood flow, temperature, biomarker tracking, etc. Under these conditions, the practice of robotic assistance by an MRI can allow an excellent IS or RDD.

2.1. Image Guided Surgical Interventions

Intraoperative imaging has fashioned a necessity to elaborate medical tools that satisfy the requests of diverse imaging techniques. Imaging backgrounds are demanding and they intensely influence the shape of the utensils used there. Advances in image resolution and disjunction capability have made interventions possible during the imaging procedure. 3D-imaging technique provides actual faithful descriptions of the human tissues while the instrument is being operated within a specified space, by tracking the coordinates of the image. In IG intraoperative procedures and MI-NI SI, MRI is increasingly more utilized due to its consistency, precision, and security. Due to its superior ability to differentiate tumor tissue from normal tissue, MRI is employed in SI for biopsies or tumor abstractions, for example [72–78]. The employed tools should be compatible with MRI. This compatibility has steered advancement of novel materials adapted for such tools. The use of an MRI-compatible robot to facilitate the approach to the body tissues inside the imaging scaffold permits the patient to remain within the scaffold during the entire SI time. Such IG association permits an important reduction of the SI duration, a higher SI accuracy, and faster recovery progression. Currently, the more accurate the IG association, the more recognizable the MRI-compatible strategies will be. Figure 3 schematically summarizes the representation of IG-SI, involving the interventional device in the MRI scaffold, the surgical data (action and location), the MRI imaging processing, and the device control.

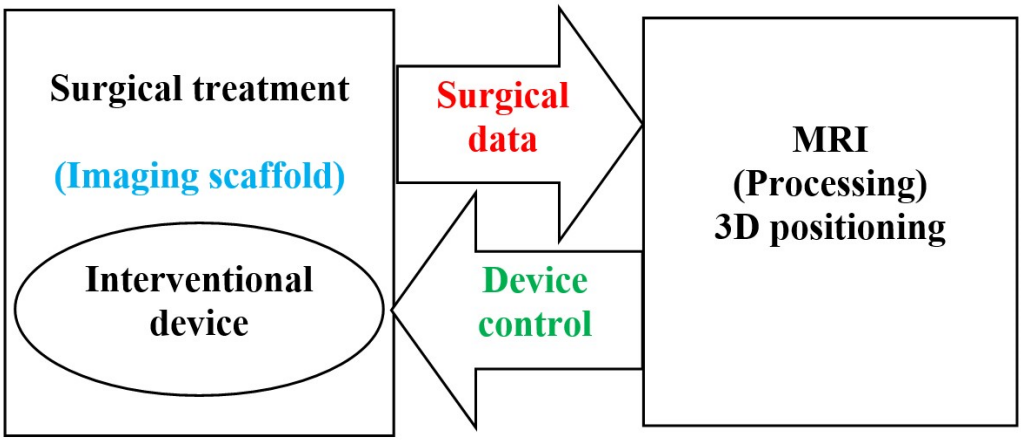

Figure 3. Schematics of an MRI IG-SI.

2.2. Implantable Drug Delivery Schemes

Operational drug delivery (DD) devices are able to deliver drugs to the target location and maintain drug intensity within a curatively relevant range. The dosage provided should deliver the drug for a specific duration necessary to achieve the greatest positive effect with the least adverse side consequences to adjacent healthy matters. Classical DD by means of discontinuous oral or intravenous delivery can result in high and rapid blood drug intensities soon after administration, thus intolerable harmful consequence may occur for patients. Another problem with these delivery modes is that they undergo first-pass metabolic rate, resulting in a significant reduction in drug concentration by the liver before attaining normal spread and hence often multiple deliveries are needed. DD made locally,

sustainably, and supervised, can have the least adverse side effects possible. The use of DD implants enables such behavior.

The most used DD schemes comprise polymer reservoir-based structures, pumps (peristaltic, infusion, and osmotic), and micro and nano electromechanical structures (MEMS and NEMS), see e.g., [79–94]. Reservoir structures utilize drug release by dispersion via a film structure. The different pumps are used according to the type of disorder, the location of the implant, and the DD permanence. Larger ones are more suited to prolonged illnesses, while smaller pumps like the osmotic pump will be more suited to local-specific particular effects using DD of uniform release. Regarding MEMS and NEMS, they behave at micro and nano levels of DD without any significant danger due to a precipitous onset of the drug.

Even though implants present sophisticated and effectual ways for controlled DD, all of them necessitate placing by medical staff. The corresponding SIs differ according to the implant location and are connected to possible defies and unfavorable outcomes. Even if side consequences are generally slight, in certain conditions they can be substantial. It may be noted that the convolution and restrictions of SI for implant placing and withdrawing have weighty influences on the technology tolerability by the patient. Intrinsically, upcoming mechanism layout should utilize MI methodologies and reduced implant sizes, and less introduction-withdrawal processes can fully influence their capacity.

Future implants could be mainstream DD methodology, if thoughtfully designed with miniature size for MI insertion and continuous DD avoiding inclusion-exclusion with ease of drug filling. In fact, all of the implants described in the last paragraph are made from non-biodegradable materials and require the disposal of SI. Two next challenges should be acknowledged: The first concerns the facilitation of self-contained implanted DD systems addressing simple and spatially homogeneous problems using constant drug release and biodegradable structures that facilitate disposal of implanted systems [60–71]. The second concerns the treatment of spatially complicated cases requiring non-uniform DD, focusing only on diseased areas and avoiding healthy areas. This requires mobile implants with actions in restricted areas. Such a problem is closely similar to that of a complex SI requiring precise spatial assistance, as the IG assistance discussed in the last section. This implanted therapy will be MI-NI-IG-RDD [42–50]. The implant structure may be of non-biodegradable material but must be MRI-compatible when using such imaging techniques [95,96]. This procedure is similar to the MI-NI-IG-SI replacing the assisted actuated-robot with an assisted actuated-RDD implant. Wireless driving and monitoring transmission entails conveying strength and signals from an outside supply to the embedded device free of physical connection [95,96]. Figure 4 shows a schematically summarized representation of an MRI IG-implanted DD, including therapeutic device (DD source) in MRI scaffold, DD data (treated zone location), MRI processing, and device control.

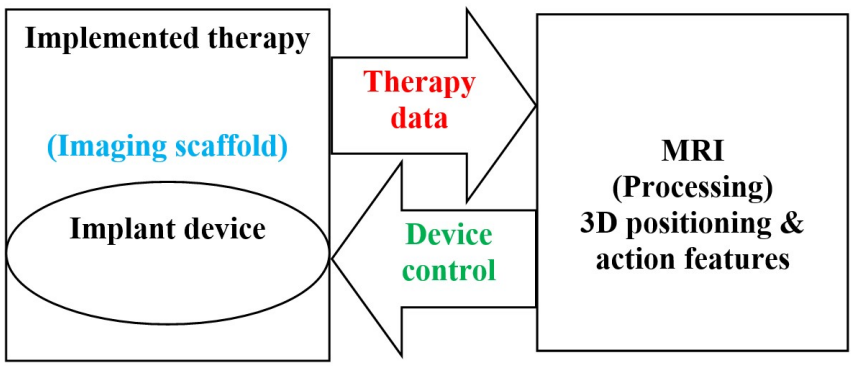

Figure 4. Summarized schematics of MRI IG-implanted DD therapeutic.

2.3. The Necessary Specifications of Surgeries and Drug Deliveries

For the well-being of patient, treatment should be precisely limited to the touched region in SI and RDD, as described in Sections 2.1 and 2.2. Such precision is associated with the actuation accuracy of the mechanism and is greatly connected to the correctness of the space tracing. Consequently, the necessary condition for such high quality topological following is the image-controlled position localization. The summary of these necessary specifications are highlighted in Figure 5.

Figure 5. Summary of requests needed for MI-IG-SI and RDD.

Such a scheme may entail a collaborative arrangement functioning self-sufficiently as shown for example in the case of RDD in Figure 6. Figure 6a shows a collaborative self-governed IG-RDD scheme including the scanner, the body troubled zone, the implant, the control system and the supply. Figure 6b illustrates two scanned brains, a safe brain, (left) and an affected brain (right) with a troubled indicated zone.

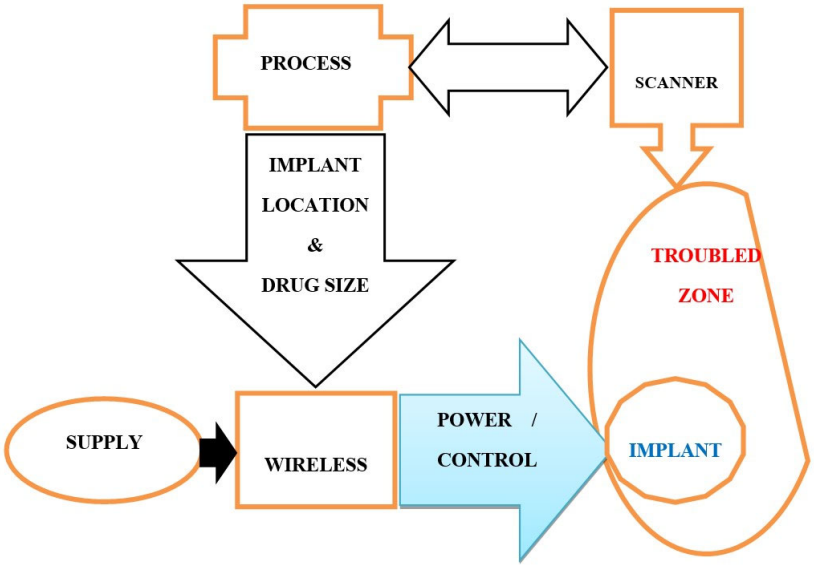

(**a**)

Figure 6. *Cont.*

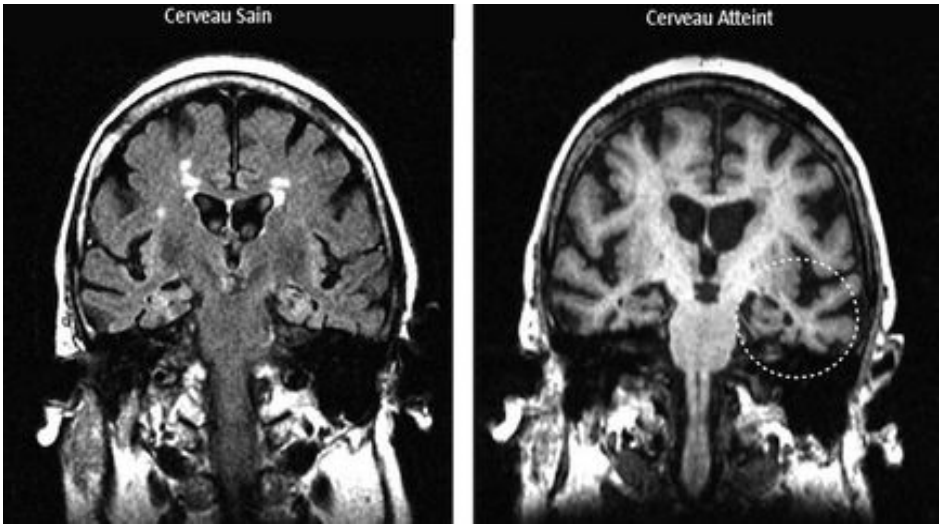

(**b**)

Figure 6. Representation of IG-RDD: (**a**) a collaborative self-governed IG-RDD scheme, (**b**) scanned safe brain (**left**), and affected brain (**right**) with a troubled indicated zone (the circle on the right side).

3. MRI Field Components

The image produced in an MRI is created by signals resulting from the interaction of magnetic fields and biological tissues. In an imaging progression, three magnetic fields of different natures are used to form 3D images. The first type is a high static field generating a magnetization vector in biological tissues aligning the tissue particles (protons) and measuring their density. The second type corresponds to three low-frequency space gradient fields locating aligned protons in tissues and forming a 3D spatial reconstruction of different tissue divisions in images. The third one is a radiofrequency field stimulating the magnetization vector to permit its detection by the scanner and the conversion of tissue assets into images [95].

Indeed, MRI, in principle, is used to image the nuclei of hydrogen atoms that are confined within the human body. A nucleus (a proton, for hydrogen), is a positive charge mass which rotates around an axis on itself. In the body tissues, protons are arbitrarily oriented and do not spin together. Consequently, they exhibit zero resultant magnetic field (the human body has no magnetization) and they perform out of phase. Reflecting the principle of MRI, protons need three essential organizations inside the explored fragment of the body tissue: to align all the protons in a fixed direction, to rotate them all together in the tissue, and to localize their distinctive origin in the space. Proton alignment could be realized by the insertion of the fragment of the body tissue in a high-strength magnet to drive them together in the axial orientation of its static magnetic field B_0. In order to achieve protons spinning together, an excitation by supplying wave radiofrequency B_1 with a frequency equal to the protons' rotation natural frequency f_L (Larmor frequency of protons) could be used allowing such action of resonance. In order to localize protons distinctive positions in the space, one may use their associated magnetic field's distinctive values. For this, a 3D space gradient G(x, y, z) with pulsations of very low-frequency repetition could be applied to the field B_0, allowing the position distinctive values of B_{0d} (x, y, z) = B_0 + G(x, y, z).

The MRI system uses three different fields, B_0, B_1, and G(x, y, z), to determine imaging of the examined fragment of the body in the following way. The value of the Larmor frequency of protons f_L is dependent of the static field value and equal to 42.5 MHz per tesla. The corresponding position distinctive values f_{Ld} (x, y, z) are functions of B_{0d} (x, y, z). An excitation of protons by radiofrequency (RF) wave energy followed by a relaxation restoring this energy permit the corresponding signal detection by a suitable tuned RF antenna coil. These signals correspond to values of B_1 of frequencies of f_{Ld} (x, y, z), which

allow coding of a spatial imaging for the concerned body part. Note that the frequency of B_1 is equal to f_L, which is usually tuned to value of f_{Ld} (x, y, z) in the center of the examined body fragment.

The three different fields employed in the MRI system are very different in nature with respect to their magnitude, frequency, and existence during system operation: B_0: 0.2–10T, 0 Hz, always present, gradient: 0–50 mT/m, 0–10 kHz, multiple pulses of few ms, B_1: 0–50 µT, 8–300 MHz, (amp. mod. pulses) of few ms. These fields are produced by the strong magnet, gradient coils, and RF coil, respectively. The most popular RF coil comes in the form of a birdcage and is used as tuned RF antenna. In conventional operation of the scanner, its correct operation requires the protection and compensation of the magnet and gradient fields. The RF field arrangement seems the most exposed and represents a weakness to noise fields and certain nearby external materials. Figure 7 shows a representation of the MRI three components and their corresponding fields.

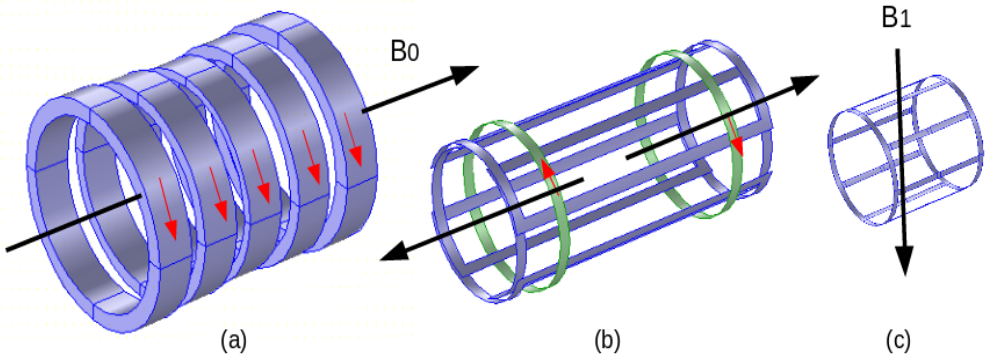

Figure 7. MRI components and fields: (**a**) electromagnet B_0, (**b**) gradient coils (one couple for one axis), (**c**) RF coil B_1.

Safety in MRI

In modern MRI schemes, one looks for briefer cycles with superior chronological and spatial resolutions. Such features seek mainly optimized performance of the **scanner** and comfort of the patient. As mentioned previously, the final image resulting from an MRI is produced by an interaction between its different fields and the biological tissues subjected to the imaging process. This interaction is at the origin of the signals converted into an image. Such an interaction may produce other undesirable effects regarding patient health or image quality. Due to these effects, understanding their behaviors is necessary for patient safety and the technical characteristics of scanner signals and images. Thus, the design of the scanner components and the realization concerns of different patient treatments could be adapted.

There are possible biological effects due to the interaction of the different magnetic fields with living tissues. We will discuss these fields successively. Theoretically, the harmless field is the static one B_0, as only body-embedded ferromagnetic matters could produce patient security troubles depending on the field strength. In general, the medical staff ponder such a problem prior to the imaging procedure. The RF field B_1 could be the most menacing for living tissues as the specific absorption rate (SAR) activated is relatively important depending on field strength and frequency. A high SAR with a long exposure duration can produce a temperature rise non-tolerated by the body [97,98]. In the case of MRI, the RF sequences are short enough and respect the limits fixed by the international safety standards [99,100]. The coils in pulsed low-frequency field gradients in MRI are constructed in such a way that the 3D gradient is uniform and can be regulated [95]. A difficult question concerns the output of the gradient involving the field strength and the rate of change of course. Shorter cycles with less imaging time can be achieved with higher gradient output. However, higher outputs may lead to disagreeable peripheral nerve stimulation (PNS) [101]. In general, PNS in this context appears not to worry the patient;

however, excessive gradient outputs can steer to life-worrying cardiac stimulation [101]. Again, the medical staff can consider such a problematic prior to the imaging procedure.

From the foregoing analysis, one can notice that optimizing the effectiveness of the MRI components, even in view of patient well-being, cannot be achieved disregarding patient security. Indeed, each case could be different and inquiring about personal data prior to treatment is essential. Note also that the interaction of the patient tissues with the different fields can cause image artifacts due to, e.g., embedded devices in the body. Considering inquired personal data, such artifacts can be counterweighed.

4. MRI-Controlled SI and RDD—Performance and Compliance

As mentioned before, the MRI system is very sensitive to EM perturbations under the form of external field noises or the introduction of certain types of material in imaging scaffold nearby the different MRI three field sources. The magnetic and conductive materials are of main concern The MRI system is typically shielded against external field noises. Regarding external materials inserted in the imaging scaffold, the static field and the gradient low frequency field are compensated and protected for slight matter introduction. For more vulnerable RF fields, it is important to control the conformity of such matter insertion.

In the case of MRI-controlled treatments, we are facing a problem relating to external matter introduction in the imaging scaffold. In such a situation, only non-magnetic and non-conductor materials can be employed. Nevertheless, in such case, we need an actuation action. Few high-performance actuators are free of non-magnetic and non-conductor materials. Piezoelectric actuators could be suitable candidates, but they need to be checked to verify their conformity, i.e., not perturbing the RF field distribution [102–111]. These actuators are composed of piezo material behaving dielectric and very thin (trivial) electrodes. The dielectric material is not supposed to perturb the field but the electrodes need to be controlled, even in the case of trivial size conductors.

4.1. Compatibility Compliance Check

We can generally characterize the MRI-compatibility of an external object as being MRI-safe, not affecting image quality, and working as expected. As mentioned before, MRI utilizes static field B_0, field gradients (position conditional field) and RF field B_1. A good MRI needs a constant uniform magnetic field B_0 (by using shimming coils) and uniform linear controlled field gradients. These fields require adjustments and compensations for consistent functioning of the scanner. The image feature can be compromised for different causes. The scanner can be the origin of reduced quality image for e.g., insufficiently shimmed. Living tissues can also reduce the image feature due to susceptibility variations e.g., between soft tissues and air holes in the brain. In addition, body embedded matters e.g., prostheses and particularly metallic ones, can also deteriorate image quality. The image alteration due to metallic materials, which present susceptibility variations, hang on the size, shape, and direction with respect to B_1. In addition, the induced currents in metals primarily by the RF field but also low-frequency gradient fields, can affect the image. The most important cause of image perturbation could be the associated tools involved in the robotic system. These could interact mainly with the RF field, which is the most vulnerable among the fields in an MRI. The main robot body and medical tools are actually constructed of non-magnetic, non-conducting materials. Different solutions are proposed for the mechatronic part of the robot involving electronics, sensors, actuators, etc., which represent a challenging compatibility question [37–41,95,96,110,112–121].

Experimental conformity control of MRI-compatibility could be achieved for existing IG installations by measuring the field perturbations due to the introduction of the tested tools inside or nearby the imaging scaffold, depending on the use of the tool. This can be conducted through sensor arrays fixed in specific positions. Such a control procedure, in the case of MRI systems, is relatively complicated (need of specific shielded chambers) and generally expensive. The field perturbation measuring tools could perturb themselves; therefore, the field and the procedure have to be managed to compensate such self-effect.

In addition, the nature of the tested tools may be unsafe and can cause damages for the **scanner** components. Moreover, such experimental control cannot be used in the design of inexistent installations. Under these conditions, an interesting solution could be a control by numerical modeling via EMC analysis to verify the MRI compatibility of the different tools [95–97,122–124].

4.2. Electromagnetic Field Perturbations

The field perturbations in a uniform electromagnetic field (EMF), due to the introduction of materials with specific characteristics, are governed by their induced EMF. The EMF equations (see the next section) are function of the next vector variables and parameters: **H** and **E** are the magnetic and electric fields, **B** and **D** are the magnetic and electric inductions, **J** is the current density, σ is the electric material conductivity, and ω is the angular frequency pulsation of the source field. The magnetic and electric comportment material laws between **B/H** and **D/E** are represented by the material permeability μ and the permittivity ε, respectively. Note that the conductor and dielectric behaviors of non-magnetic matters are dependent on the frequency following the relative values of σ and ω.ε in the relation $\mathbf{J} = \sigma\,\mathbf{E} + j\,\omega\,\mathbf{D}$ such that when $\sigma >> \omega.\varepsilon$, the behavior is mainly a conductor, and for $\sigma << \omega.\varepsilon$, it is mainly dielectric. In the RF range, the above-mentioned electrodes in piezoelectric actuators belong to the first category and the piezoelectric material to the second, respectively.

4.3. EMC Conformity Control

The EMC analysis aims to control the influence of hosting in the MRI atmosphere diverse stuffs employed in medical treatments. Intended for EMC analysis, we can reflect expressions (1)–(4) that give the EMF equations:

$$\boldsymbol{\nabla} \times \mathbf{H} = \mathbf{J} \tag{1}$$

$$\mathbf{J} = \sigma\,\mathbf{E} + j\,\omega\,\mathbf{D} + \mathbf{Je} \tag{2}$$

$$\mathbf{E} = -\,\boldsymbol{\nabla}\,V - j\,\omega\,\mathbf{A} \tag{3}$$

$$\mathbf{B} = \boldsymbol{\nabla} \times \mathbf{A} \tag{4}$$

In the EMF Equations (1)–(4), **H**, **E**, **B**, **D**, and **J** have been defined before, **A** and V are the magnetic vector and electric scalar potentials. $\mathbf{J_e}$ the source current density. The parameters σ, ω, μ, and ε have been defined before. The symbol $\boldsymbol{\nabla}$ is a vector of partial derivative operators, and its three possible implications are gradient (product with a scalar field), divergence and curl (dot and cross products, respectively, with a vector field). The Input source term in EMF Equations (1)–(4) is $\mathbf{J_e}$ or its equivalent electric field $\sigma\,\mathbf{E_e}$.

The ruling Equations (1)–(4) can be solved locally in the birdcage RF coil-antenna for reference conditions (without inserted matter) compared to situations involving the diverse controlled matters. This can be accomplished by means of numerical discretized methods [125–131] or other techniques allowing local computations.

The magnetic compatibility of a material is characterized by its permeability $\mu\ (=\mu_0.\ \mu_r)$ or the susceptibility $\chi\ (=\mu_r - 1)$. For a high magnetic material, $\mu_r >> 1$ and $\mu_r \approx \chi$. For non-magnetic material, $\mu_r = 1$ and $\chi = 0$. Thus, a magnetic material that is MRI-compatible has $\mu_r \approx 1$, or $\chi \approx 0$. In addition, the conductivity σ characterizes the electric compatibility of a material, so an electric conductor that MRI-compatible has $\sigma \approx 0$. Therefore, a completely MRI-compatible material has zero values for both χ and σ. In practice, a magnetic field as B_1 could be perturbed by the introduction of a magnetic material with non-zero value of χ and indirectly due to eddy currents induced in a material introduced in the imaging scaffold having a non-zero value of σ.

Note that these perturbations depend on the size, the shape, and the orientation of the introduced matter as well as the frequency of the field (as will be demonstrated in the next example).

4.4. Application Example

Let us consider a simple example illustrating the mentioned methodology for checking the compliance of the materials inserted into the birdcage coil positioned in the tunnel of an MRI. The corresponding case geometry involves a 30 cm diameter and 30 cm length birdcage coil-antenna located in a 60 cm diameter tunnel. The tested matters have a form of a cube with 5 cm side (125 cm^3) embedded in the center of the birdcage coil. A RF field in the birdcage coil at 63.87 MHz corresponds to the frequency f_L (for a value of B_0 of 1.5 T) tuned to the value in the center of the considered geometry. The corresponding RF field distribution in the tunnel can be computed for the reference case (without tested matter) and for the different cases, involving tested matters in the studied scheme. Computations are based on 3D discretization of the field **E** using edge finite elements with appropriate boundary conditions. Figure 8 illustrates the RF field distribution in the reference case.

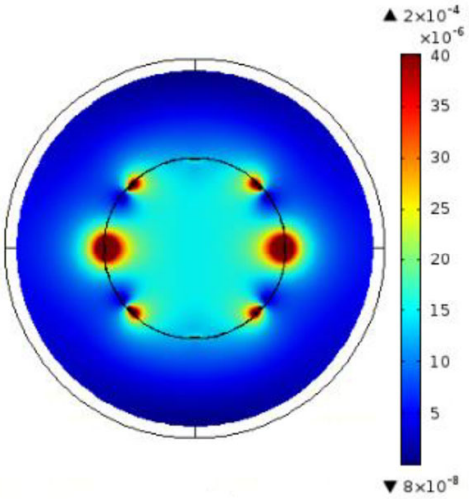

Figure 8. RF magnetic field (vertically directed) distribution in the axial cross section of the birdcage inside the tunnel. Reference case: no material.

We will illustrate now the case of piezoelectric actuation involving piezo material coated on two opposite faces by very thin electrodes. The characteristics of the piezo are $\mu_r = 1.0$, $\varepsilon_r = [450°990°990]$, $\sigma = 0$ S/m. Note that the relative permittivity is given by an anisotropic vector where the value in polarization direction is less than in the other two directions. The electrodes conductors are characterized as $\mu_r = 1.0$, $\varepsilon_r = 1.0$, $\sigma = 3.77 \times 10^7$ S/m.

Since the currents induced by a field develop in the section of the conductor perpendicular to the direction of the field, we can consider the following two opposite cases. Field distributions were calculated for both situations of electrodes perpendicular and parallel to the direction of the field. Figure 9 displays the field distributions for both cases. The results confirmed that the orientation of the electrodes and hence the actuator (evoked in Section 4.3) plays an important role. The influence of the conducting electrode can be considerably reduced if it is parallel to the field. Note that Figure 9c shows almost the same field distributions as Figure 8.

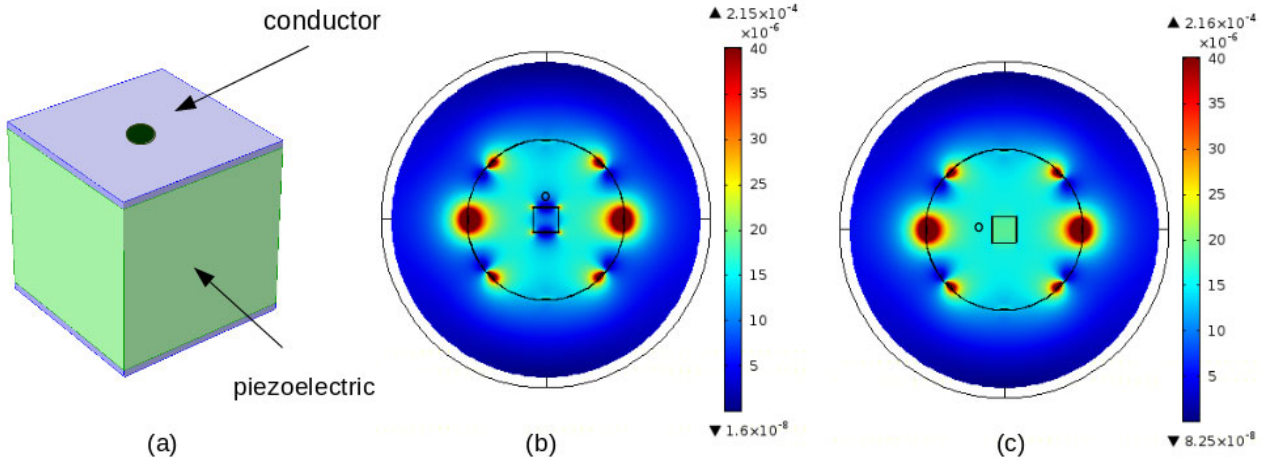

Figure 9. Distribution of RF magnetic field (vertical) in piezoelectric coated by thin electrodes case: (**a**) structure arrangement, (**b**) electrodes perpendicular to the field, (**c**) electrodes parallel to the field.

Notice that the field distributions of Figures 8 and 9 are reached for equal input conditions; consequently, they can offer a behavioral evocation. At that point, the present EMC analysis in MRI light up a procedure for checking any disturbs through image-guided maneuvers.

5. Discussion

In this manuscript, the analysis and evaluation carried out on image-guided procedures of surgical interventions and restricted delivery of implanted drugs under minimally invasive and non-ionizing circumstances have illustrated that such a topic is totally beneficial. At this stage, various questions deserve to be raised:

To know how to go further in the well-being of the patient and allow the medical team to verify new therapies and even to carry out treatment training without risk for the patient, we can use physical copies of the real patient. This helps elucidate the treatment most suited to the actual patient. This can be conducted on different levels. The use of a physical phantom built of materials corresponding to the real body biological properties in the IG, SI, and RDD automated procedures (see Figures 3, 4 and 6) reflects the simplest level.

A more sophisticated level corresponds to the practice of a matching process of the physical phantom treatment process and a virtual replica of such process. Such a twin of real-virtual procedure permits a self-corrected behavior. The real part delivers sensor-processed data to the virtual side and the last forward-control instructions issued from the mathematical model of the real part. This matching procedure allows mastering all undesired and hazarded functioning phenomena. The matching real-virtual twin uses the concept of digital twin (DT), [132]. Such a concept exists and is practiced in different industrial fields [133–135]. Figure 10 illustrates schematically the DT concept in the case of medical procedures assisted by imaging IG. The real part includes the complex medical procedure involving the scanner, the robot, and body phantom. The virtual side comprises the digital procedure model involving the digital body phantom. The matching link in between these two sides include sensing, control, and processes.

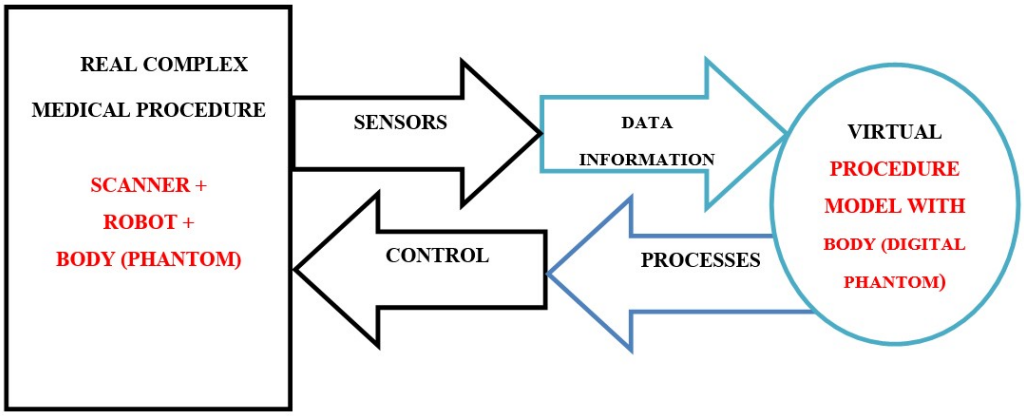

Figure 10. Schematic representation of the DT concept for IG medical treatments.

The superior level of using IG medical treatments regards real procedures of DT involving the real patient. Moreover, this matching twin could be amended with "Human-in-the-loop" approaches permitting the supervision, the control, and the correction of its functioning; we will call such twins HDTs.

The DT concept is gradually entering the healthcare field using virtual replicas of physical individuals that go beyond a static image integrating the dynamic behavior of a real living individual [136–146]. Human–robot interaction associated with DT allows higher control of IG, SI, and RDD, minimizing risk for the patient [147–149]. The quality of the body model plays an important role in matching behavior; see for example [150–153]. One of the important challenges is real-time modeling of tissues, with distortion and development that resemble reality. DT and HDT potentially revolutionize the treatment, investigation and training of IG, SI, and RDD. Despite its capabilities, medical treatment is still in its beginning in terms of its ability to represent human tissue in a living, real-time digital replica.

Furthermore, to go beyond, the involvement of artificial intelligence (AI) practices in these medical treatments contributes to reducing the complexity of information acquisition and post-processing in MRI through the use of strategy acceleration and offering faster analysis times with easier image processing [145,154]. AI can be used also to execute planed recurrent training jobs in IG robots.

This can be profusely enlarged by using increased interaction of human and robot advancing the global system performing through augmented reality (AR)-assisted robotic operations. AR associated to IG-MRI in complex procedures can allow significant reduction of hazards like tissue damage, bleeding, post-operative trauma, etc. In addition, DT can play an important role in AR-assisted robotic operations regarding patient-adapted treatment. This permits determination of precisely the disorder source and required action utilizing patient individual modeling from deep learning databases. Moreover, the association AR-DT allows an important accuracy in the domain of suturing, tying, and placement contrasted to hand operations [155–159].

6. Conclusions

In this paper, the assessment of image-guided procedures of surgical interventions and implanted restricted drug delivery under minimally invasive and non-ionizing circumstances has been realized. Analysis of the different concerns confronted in this review has revealed that there is an incessant progress in this domain. The matters of significance erected by this topic are various, the most significant of which are summarized as follows.

The universal goals of medical treatments could be to go further in the well-being of the patient and to allow medical personnel to test new therapies and carry out therapeutic training without risk to the patient. Due to these purposes, different strategic aids can be requested in healthcare:

- Image-assisted robotics, non-ionized, minimally invasive, and locally restrictive means;
- Physical phantoms based on the actual biological properties of the body;
- Digital twins under human control;
- Artificial intelligence tools and robotics assisted by augmented reality.

The specific challenges on this topic fall into two categories. The first is linked to the operation of the robotic assistance by the scanner, which can be improved using augmented reality and artificial intelligence tools. The second concerns the complete automation, conditioned on patient safety, of image-guided procedures, which can be carried out by digital twins controlled by humans in real time. This may enable more precise, minimally invasive restrictive actions with the possibility of strict human observational control.

One of the most difficult problems concerns the behavior of tissues in real time in virtual simulations, which is needed among others in matching of real–virtual twins. This problem faces different difficulties, computational complexities, tedious tasks relating to the calculation time and real-time matching speed required. The main cause of these difficulties is the non-linearity of biological tissues reflecting complex constitutive laws representing the deformation and displacement behaviors of elastic tissues. Either approximate constitutive laws, adapted computational techniques, or a combined methodology could address this open research problem.

Funding: This research received no external funding.

Institutional Review Board Statement: Not applicable.

Informed Consent Statement: Not applicable.

Data Availability Statement: Not applicable.

Conflicts of Interest: The author declares no conflict of interest.

References

1. Reiss, S.; Wäscher, K.; Caglar Özen, A.; Lottner, T.; Heidt, T.; von Zur Mühlen, C.; Bock, M. Quantifying myocardial perfusion during MR-guided interventions without exogenous contrast agents: Intra-arterial spin labeling. *Z. Med. Phys.* **2023**. *in print*. [CrossRef] [PubMed]
2. Huang, S.; Lou, C.; Zhou, Y.; He, Z.; Jin, X.; Feng, Y.; Anzhu Gao, A.; Yang, G.Z. MRI-guided robot intervention—Current state-of-the-art and new challenges. *Med-X* **2023**, *1*, 4. [CrossRef]
3. Faoro, G.; Maglio, S.; Pane, S.; Iacovacci, V.; Menciassi, A. An Artificial Intelligence-Aided Robotic Platform for Ultrasound-Guided Transcarotid Revascularization. *IEEE Robot. Autom. Lett.* **2023**, *8*, 2349–2356. [CrossRef]
4. Morris, E.D.; O'Connell, D.P.; Gao, Y.; Cao, M. MR safety considerations for MRI-guided radiotherapy. In *Advances in Magnetic Resonance Technology and Applications*; Academic Press: Cambridge, MA, USA, 2022; Volume 8, pp. 81–100. [CrossRef]
5. Su, H.; Kwok, K.W.; Cleary, K.; Iordachita, I.; Cavusoglu, M.C.; Desai, J.P.; Fischer, G.S. State of the art and future opportunities in MRI-guided robot-assisted surgery and interventions. *Proc. IEEE* **2022**, *110*, 968–992. [CrossRef] [PubMed]
6. Padhan, J.; Tsekos, N.; Al-Ansari, A.; Abinahed, J.; Deng, Z.; Navkar, N.V. Dynamic Guidance Virtual Fixtures for Guiding Robotic Interventions: Intraoperative MRI-guided Transapical Cardiac Intervention Paradigm. In Proceedings of the 2022 IEEE 22nd International Conference on Bioinformatics and Bioengineering (BIBE), Taichung, Taiwan, 7–9 November 2022; pp. 265–270. [CrossRef]
7. Singh, S.; Torrealdea, F.; Bandula, S. MR Imaging—Guided Intervention: Evaluation of MR Conditional Biopsy and Ablation Needle Tip Artifacts at 3T Using a Balanced Fast Field Echo Sequence. *J. Vasc. Interv. Radiol.* **2021**, *32*, 1068–1074. [CrossRef] [PubMed]
8. Kuah, T.; Vellayappan, B.A.; Makmur, A.; Nair, S.; Song, J.; Tan, J.H.; Kumar, N.; Quek, S.T. State-of-the-Art Imaging Techniques in Metastatic Spinal Cord Compression. *Cancers* **2022**, *14*, 3289. [CrossRef] [PubMed]
9. Kraus, M.S.; Coblentz, A.C.; Deshpande, V.S.; Peeters, J.M.; Itriago-Leon, P.M.; Chavhan, G.B. State-of-the-art magnetic resonance imaging sequences for pediatric body imaging. *Pediatr. Radiol.* **2023**, *53*, 1285–1299. [CrossRef]
10. Attenberger, U.I.; Biber, S.; Wichtmann, B.D. Technological Advances of Magnetic Resonance Imaging in Today's Health Care Environment. *Investig. Radiol.* **2020**, *55*, 531–542. [CrossRef]
11. Sennimalai, K.; Selvaraj, M.; Kharbanda, O.P.; Kandasamy, D.; Mohaideen, K. MRI-based cephalometrics: A scoping review of current insights and future perspectives. *Dentomaxillofac. Radiol.* **2023**, *52*, 20230024. [CrossRef]
12. Chianca, V.; Vincenzo, B.; Cuocolo, R.; Zappia, M.; Guarino, S.; Di Pietto, F.; Del Grande, F. MRI Quantitative Evaluation of Muscle Fatty Infiltration. *Magnetochemistry* **2023**, *9*, 111. [CrossRef]

13. Wang, X.; Guo, S.; Li, Z.; Luo, Q.; Dai, Y.; Zhang, H.; Ye, Y.; Gong, Q.; Luo, K. Amphiphilic branched polymer-nitroxides conjugate as a nanoscale agent for potential magnetic resonance imaging of multiple objects in vivo. *J. Nanobiotechnol.* **2021**, *19*, 205. [CrossRef] [PubMed]
14. Sato, Y.; Takeuchi, T.; Fuju, A.; Takahashi, M.; Hashimoto, M.; Okawa, R.; Hayashi, N. MRI safety for leave-on powdered hair thickeners under 1.5-T and 3.0-T MRI: Measurement of deflection force, MRI artifact, and evaluation of preexamination screening. *Phys. Eng. Sci. Med.* **2023**, *46*, 915–924. [CrossRef] [PubMed]
15. Akdogan, G.; Istanbullu, O. Analysing the effects of metallic biomaterial design and imaging sequences on MRI interpretation challenges due to image artefacts. *Phys. Eng. Sci. Med.* **2022**, *45*, 1163–1174. [CrossRef] [PubMed]
16. Germann, C.; Nanz, D.; Sutter, R. Magnetic Resonance Imaging Around Metal at 1.5 Tesla: Techniques from Basic to Advanced and Clinical Impact. *Investig. Radiol.* **2021**, *56*, 734–748. [CrossRef] [PubMed]
17. Germann, C.; Falkowski, A.L.; von Deuster, C.; Nanz, D.; Sutter, R. Basic and Advanced Metal-Artifact Reduction Techniques at Ultra-High Field 7-T Magnetic Resonance Imaging-Phantom Study Investigating Feasibility and Efficacy. *Investig. Radiol.* **2022**, *57*, 387–398. [CrossRef] [PubMed]
18. Inaoka, T.; Kitamura, N.; Sugeta, M.; Nakatsuka, T.; Ishikawa, R.; Kasuya, S.; Sugiura, Y.; Nakajima, A.; Nakagawa, K.; Terada, H. Diagnostic Value of Advanced Metal Artifact Reduction Magnetic Resonance Imaging for Periprosthetic Joint Infection. *J. Comput. Assist. Tomogr.* **2022**, *46*, 455–463. [CrossRef] [PubMed]
19. Haskell, M.W.; Nielsen, J.F.; Noll, D.C. Off-resonance artifact correction for MRI: A review. *NMR Biomed.* **2023**, *36*, e4867. [CrossRef]
20. Spronk, T.; Kraff, O.; Kreutner, J.; Schaefers, G.; Quick, H.H. Development and evaluation of a numerical simulation approach to predict metal artifacts from passive implants in MRI. *Magma* **2022**, *35*, 485–497. [CrossRef]
21. Hu, Q.; Yu, V.Y.; Yang, Y.; Hu, P.; Sheng, K.; Lee, P.P.; Kishan, A.U.; Raldow, A.C.; O'Connell, D.P.; Woods, K.E.; et al. Practical Safety Considerations for Integration of Magnetic Resonance Imaging in Radiation Therapy. *Pract. Radiat. Oncol.* **2020**, *10*, 443–453. [CrossRef]
22. Hu, Q.; Yu, V.Y.; Yang, Y.; Hu, P.; Sheng, K.; Lee, P.P.; Kishan, A.U.; Raldow, A.C.; O'Connell, D.P.; Woods, K.E.; et al. Rapid safety assessment and mitigation of radiofrequency induced implant heating using small root mean square sensors and the sensor matrix Q_s. *Magn. Reason. Med.* **2022**, *87*, 509–527. [CrossRef]
23. Fierens, G.; Standaert, N.; Peeters, R.; Glorieux, C.; Verhaert, N. Safety of active auditory implants in magnetic resonance imaging. *J. Otol.* **2021**, *16*, 185–198. [CrossRef] [PubMed]
24. Peschke, E.; Ulloa, P.; Jansen, O.; Hoevener, J.B. Metallic Implants in MRI—Hazards and Imaging Artifacts. *Met. Implant. MRT Gefahren Bildartefakte. Rofo.* **2021**, *193*, 1285–1293. [CrossRef] [PubMed]
25. Lu, M.; Zhang, Y.; Du, H. Design and control of a novel magnetic resonance imaging-compatible breast intervention robot. *Int. J. Adv. Robot. Syst.* **2020**, *17*, 1729881420927853. [CrossRef]
26. Carter, L.N.; Addison, O.; Naji, N.; Seres, P.; Wilman, A.H.; Shepherd, D.E.T.; Grover, L.; Cox, S. Reducing MRI susceptibility artefacts in implants using additively manufactured porous Ti-6Al-4V structures. *Acta Biomater.* **2020**, *107*, 338–348. [CrossRef] [PubMed]
27. Khodarahmi, I.; Brinkmann, I.M.; Lin, D.J.; Bruno, M.; Johnson, P.M.; Knoll, F.; Keerthivasan, M.B.; Chandarana, H.; Fritz, J. New-Generation Low-Field Magnetic Resonance Imaging of Hip Arthroplasty Implants Using Slice Encoding for Metal Artifact Correction: First In Vitro Experience at 0.55 T and Comparison with 1.5 T. *Investig. Radiol.* **2022**, *57*, 517–526. [CrossRef] [PubMed]
28. Lee, E.M.; Ibrahim, E.S.H.; Dudek, N.; Lu, J.C.; Kalia, V.; Runge, M.; Srinivasan, A.; Stojanovska, J.; Agarwal, P.P. Improving MR image quality in patients with metallic implants. *Radiographics* **2021**, *41*, 126–137. [CrossRef] [PubMed]
29. Manso Jimeno, M.; Vaughan, J.T.; Geethanath, S. Superconducting magnet designs and MRI accessibility: A review. *NMR Biomed.* **2023**, *36*, e4921. [CrossRef]
30. Amin, N.; Pai, I.; Touska, P.; Connor, S.E.J. Utilization of SEMAC-VAT MRI for Improved Visualization of Posterior Fossa Structures in Patients with Cochlear Implants. *Otol. Neurotol.* **2021**, *42*, 451–458. [CrossRef]
31. Kumar, N.; Alathur Ramakrishnan, S.; Lopez, K.G.; Wang, N.; Madhu, S.; Vellayappan, B.A.; Hallinan, J.T.P.D.; Fuh, J.Y.H.; Kumar, A.S. Design and 3D printing of novel titanium spine rods with lower flexural modulus and stiffness profile with optimised imaging compatibility. *Eur. Spine J.* **2023**, *32*, 1953–1965. [CrossRef]
32. Rajiah, P.S.; François, C.J.; Leiner, T. Cardiac MRI: State of the Art. *Radiology* **2023**, *307*, e223008. [CrossRef]
33. Basit, A.; Inam, O.; Omer, H. Accelerating GRAPPA reconstruction using SoC design for real-time cardiac MRI. *Comput. Biol. Med.* **2023**, *160*, 107008. [CrossRef] [PubMed]
34. Zolfaghari, P.; Erden, O.K.; Ferhanoglu, O.; Tümer, M.; Yalcinkaya, A.D. MRI Compatible Fiber Optic Multi Sensor Platform for Real Time Vital Monitoring. *J. Light. Technol.* **2021**, *39*, 4138–4144. [CrossRef]
35. Wang, F.; Qi, H.; De Goyeneche, A.; Heckel, R.; Lustig, M.; Shimron, E. K-band: Self-supervised MRI Reconstruction via Stochastic Gradient Descent over K-space Subsets. *arXiv* **2023**, arXiv:2308.02958. [CrossRef]
36. Lee, K.-H.; Fu, K.C.D.; Guo, Z.; Dong, Z.; Leong, M.C.W.; Cheung, C.L.; Lee, A.P.W.; Luk, W.; Kwok, K.W. MR Safe Robotic Manipulator for MRI-Guided Intracardiac Catheterization. *IEEE ASME Trans. Mechatron.* **2018**, *23*, 586–595. [CrossRef]
37. Farooq, M.U.; Ko, S.Y. A Decade of MRI Compatible Robots: Systematic Review. *Trans. Robot.* **2023**, *39*, 862–884. [CrossRef]
38. Farooq, M.U.; Ko, S.Y.; Seung, S.; Kim, C.; Cha, K.; Oh, S.S.; You, H. An MRI-compatible endonasal surgical robotic system: Kinematic analysis and performance evaluation. *Mechatronics* **2023**, *94*, 103029. [CrossRef]

39. Manjila, S.; Rosa, B.; Price, K.; Manjila, R.; Mencattelli, M.; Dupont, P.E. Robotic Instruments Inside the MRI Bore: Key Concepts and Evolving Paradigms in Imaging-enhanced Cranial Neurosurgery. *World Neurosurg.* **2023**, *176*, 127–139. [CrossRef]
40. Zhao, Z.; Carvalho, P.A.; Tang, H.; Pooladvand, K.; Gandomi, K.Y.; Nycz, C.J.; Furlong, C.; Fischer, G.S. Preliminary Characterization of a Plastic Piezoelectric Motor Stator Using High-Speed Digital Holographic Interferometry. In *Advancement of Optical Methods & Digital Image Correlation in Experimental Mechanics. Conference Proceedings of the Society for Experimental Mechanics Series*; Lin, M.T., Furlong, C., Hwang, C.H., Eds.; Springer: Cham, Switzerland, 2021. [CrossRef]
41. Carvalho, P.A.; Tang, H.; Razavi, P.; Pooladvand, K.; Castro, W.C.; Gandomi, K.Y.; Zhao, Z.; Nycz, C.J.; Furlong, C.; Fischer, G.S. Study of MRI Compatible Piezoelectric Motors by Finite Element Modeling and High-Speed Digital Holography. In *Advancement of Optical Methods & Digital Image Correlation in Experimental Mechanics. Conference Proceedings of the Society for Experimental Mechanics Series*; Lin, M.T., Furlong, C., Hwang, C.H., Eds.; Springer: Cham, Switzerland, 2020. [CrossRef]
42. Williams, R.P.; Karzova, M.M.; Yuldashev, P.V.; Kaloev, A.Z.; Nartov, F.A.; Khokhlova, V.A.; Cunitz, B.W.; Morrison, K.P.; Khokhlova, T.D. Dual-Mode 1-D Linear Ultrasound Array for Image-Guided Drug Delivery Enhancement without Ultrasound Contrast Agents. *IEEE Trans. Ultrason. Ferroelectr. Freq. Control* **2023**, *70*, 693–707. [CrossRef]
43. Williams, R.P.; Karzova, M.M.; Yuldashev, P.V.; Kaloev, A.Z.; Nartov, F.A.; Khokhlova, V.A.; Cunitz, B.W.; Morrison, K.P.; Khokhlova, T.D. Microbubble-mediated ultrasound drug-delivery and therapeutic monitoring. *Expert Opin. Drug Deliv.* **2017**, *14*, 1031–1043. [CrossRef]
44. Delaney, L.J.; Isguven, S.; Eisenbrey, J.R.; Hickok, N.J.; Forsberg, F. Making waves: How ultrasound-targeted drug delivery is changing pharmaceutical approaches. *Mater. Adv.* **2022**, *3*, 3023–3040. [CrossRef]
45. Nazary Abrbekoh, F.; Salimi, L.; Saghati, S.; Amini, H.; Fathi Karkan, S.; Moharamzadeh, K.; Sokullu, E.; Rahbarghazi, R. Application of microneedle patches for drug delivery; doorstep to novel therapies. *J. Tissue Eng.* **2022**, *13*, 20417314221085390. [CrossRef]
46. Arno, M.C.; Simpson, J.D.; Blackman, L.D.; Brannigan, R.P.; Thurecht, K.J.; Dove, A.P. Enhanced drug delivery to cancer cells through a pH-sensitive polycarbonate platform. *Biomater. Sci.* **2023**, *11*, 908–915. [CrossRef] [PubMed]
47. Chen, W.; Cheng, C.A.; Zink, J.I. Spatial, temporal, and dose control of drug delivery using noninvasive magnetic stimulation. *ACS Nano* **2019**, *13*, 1292–1308. [CrossRef] [PubMed]
48. Huang, J.; Xiao, K. Nanoparticles-based strategies to improve the delivery of therapeutic small interfering RNA in precision oncology. *Pharmaceutics* **2022**, *14*, 1586. [CrossRef]
49. Jia, M.; Zhang, D.; Zhang, C.; Li, C. Nanoparticle-based delivery systems modulate the tumor microenvironment in pancreatic cancer for enhanced therapy. *J. Nanobiotechnol.* **2021**, *19*, 384. [CrossRef]
50. Zhao, J.F.; Zou, F.L.; Zhu, J.F.; Huang, C.; Bu, F.; Zhu, Z.; Yuan, R. Nano-drug delivery system for pancreatic cancer: A visualization and bibliometric analysis. *Front. Pharmacol.* **2022**, *13*, 1025618. [CrossRef] [PubMed]
51. Espiritu, J.; Berangi, M.; Yiannakou, C.; Silva, E.; Francischello, R.; Kuehne, A.; Niendorf, T.; Könneker, S.; Willumeit-Römer, R.; Seitz, J.M. Evaluating metallic artefact of biodegradable magnesium-based implants in magnetic resonance imaging. *Bioact. Mater.* **2022**, *15*, 382–391. [CrossRef] [PubMed]
52. Fritz, J.; Rashidi, A.; de Cesar Netto, C. Magnetic Resonance Imaging of Total Ankle Arthroplasty: State-of-The-Art Assessment of Implant-Related Pain and Dysfunction. *Foot Ankle Clin.* **2023**, *28*, 463–492. [CrossRef]
53. Berangi, M.; Kuehne, A.; Waiczies, H.; Niendorf, T. MRI of Implantation Sites Using Parallel Transmission of an Optimized Radiofrequency Excitation Vector. *Tomography* **2023**, *9*, 603–620. [CrossRef]
54. Canzi, P.; Magnetto, M.; Simoncelli, A.; Manfrin, M.; Aprile, F.; Lafe, E.; Carlotto, E.; Avato, I.; Scribante, A.; Preda, L.; et al. The role of cochlear implant positioning on MR imaging quality: A preclinical in vivo study with a novel implant magnet system. *Eur. Arch. Otorhinolaryngol.* **2022**, *279*, 2889–2898. [CrossRef]
55. Kimura, M.; Kaku, N.; Kubota, Y.; Tagomori, H.; Tsumura, H. Fluorodeoxyglucose Positron-Emission Tomography/Computed Tomography and Magnetic Resonance Imaging for Adverse Local Tissue Reactions near Metal Implants after Total Hip Arthroplasty: A Preliminary Report. *Clin. Orthop. Surg.* **2021**, *13*, 320–328. [CrossRef] [PubMed]
56. Fierens, G.; Walraevens, J.; Peeters, R.; Glorieux, C.; Verhaert, N. Metal artefact reduction sequences for a piezoelectric bone conduction implant using a realistic head phantom in MRI. *arXiv* **2023**, arXiv:2306.03767. [CrossRef]
57. Winchester, A.; Kay-Rivest, E.; Bruno, M.; Hagiwara, M.; Moonis, G.; Jethanamest, D. Image Quality and Artifact Reduction of a Cochlear Implant with Rotatable Magnets. *Otol. Neurotol.* **2023**, *44*, e223–e229. [CrossRef] [PubMed]
58. Vuorinen, A.-M. Magnetic Resonance Imaging in Patients with Cardiac Implantable Electronic Devices: Safety and Image Quality. Ph.D. Thesis, University of Helsinki, Helsinki, Finland, 2023. Available online: https://helda.helsinki.fi/bitstream/handle/10138/352340/Vuorinen_Aino-Maija_dissertation2023.pdf?sequence=1&isAllowed=y (accessed on 1 November 2023).
59. Canzi, P.; Carlotto, E.; Simoncelli, A.M.; Lafe, E.; Minervini, D.; Balzi, D.; Delasio, A.; Malpede, S.; Robotti, C.; Manfrin, M.; et al. Recent advances in managing MRI artifacts caused by auditory implants: The effect of Metal Artifact Reduction Sequences. *Audiol. Foniatr.* **2022**, *7*, 25–33. [CrossRef]
60. Traverson, M.; Heiden, M.; Stanciu, L.A.; Nauman, E.A.; Jones-Hall, Y.; Breur, G.J. In Vivo Evaluation of Biodegradability and Biocompatibility of Fe30Mn Alloy. *Vet. Comp. Orthop. Traumatol.* **2018**, *31*, 10–16. [CrossRef] [PubMed]
61. Wang, Y.; Venezuela, J.; Dargusch, M. Biodegradable shape memory alloys: Progress and prospects. *Biomaterials* **2021**, *279*, 121215. [CrossRef] [PubMed]

62. Li, H.; Lin, G.; Wang, P.; Huang, J.; Wen, C. Nutrient alloying elements in biodegradable metals: A review. *J. Mater. Chem. B* **2021**, *9*, 9806–9825. [CrossRef]
63. Rabeeh, V.P.M.; Hanas, T. Progress in manufacturing and processing of degradable Fe-based implants: A review. *Prog. Biomater.* **2022**, *11*, 163–191. [CrossRef]
64. Babacan, N.; Kochta, F.; Hoffmann, V.; Gemming, T. Effect of silver additions on the microstructure, mechanical properties and corrosion behavior of biodegradable Fe-30Mn-6Si. *Mater. Today Commun.* **2021**, *28*, 102689. [CrossRef]
65. Tai, C.-C.; Lo, H.-L.; Liaw, C.-K.; Huang, Y.-M.; Huang, Y.-H.; Yang, K.-Y.; Huang, C.-C.; Huang, S.-I.; Shen, H.-H.; Lin, T.-H.; et al. Biocompatibility and Biological Performance Evaluation of Additive-Manufactured Bioabsorbable Iron-Based Porous Suture Anchor in a Rabbit Model. *Int. J. Mol. Sci.* **2021**, *22*, 7368. [CrossRef]
66. Bakhsheshi-Rad, H.R.; Najafinezhad, A.; Hadisi, Z.; Iqbal, N. Characterization and biological properties of nanostructured clinoenstatite scaffolds for bone tissue engineering applications. *Mater. Chem. Phys.* **2021**, *259*, 123969. [CrossRef]
67. Sun, Y.; Chen, L.; Liu, N.; Wang, H.; Liang, C. Laser-modified fe–30 mn surfaces with promoted biodegradability and biocompatibility toward biological applications. *J. Mater. Sci.* **2021**, *56*, 13772–13784. [CrossRef]
68. Saliba, L.; Sammut, K.; Tonna, C.; Pavli, F. FeMn and FeMnag Biodegradable Alloys: An In Vitro and In Vivo Investigation. Available online: https://ssrn.com/abstract=4325636 (accessed on 1 November 2023). [CrossRef]
69. Hao, S.; Yang, T.; Zhang, A.; Wang, P.; Jiang, H.; Shen, D.; Guo, L.; Ye, M. Evaluation of Biodegradable Alloy Fe30Mn0.6N in Rabbit Femur and Cartilage through Detecting Osteogenesis and Autophagy. *Biomed Res. Int.* **2023**, *18*, 3626776. [CrossRef] [PubMed]
70. Biffi, C.A.; Fiocchi, J.; Bregoli, C.; Gambaro, S.; Copes, F.; Mantovani, D.; Tuissi, A. Ultrashort Laser Texturing for Tuning Surface Morphology and Degradation Behavior of the Biodegradable Fe–20Mn Alloy for Temporary Implants. *Adv. Eng. Mater.* **2022**, *24*, 2101496. [CrossRef]
71. Putra, N.E.; Leeflang, M.A.; Taheri, P.; Fratila-Apachitei, L.E.; Mol, J.M.C.; Zhou, J.; Zadpoor, A.A. Extrusion-based 3D printing of ex situ-alloyed highly biodegradable MRI-friendly porous iron-manganese scaffolds. *Acta Biomater.* **2021**, *134*, 774–790. [CrossRef] [PubMed]
72. Jia, X.; Zhang, Y.; Du, H.; Yu, Y. Experimental Study of Double Cable-Conduit Driving Device for Mri Compatible Biopsy Robots. *J. Mech. Med. Biol.* **2021**, *21*, 2140014. [CrossRef]
73. Li, X.; Young, A.S.; Raman, S.S.; Lu, D.S.; Lee, Y.H.; Tsao, T.C.; Wu, H.H. Automatic needle tracking using Mask R-CNN for MRI-guided percutaneous interventions. *Int. J. Comput. Assist. Radiol. Surg.* **2020**, *15*, 1673–1684. [CrossRef]
74. Publicover, J.; Gallop, D.; Elliott, C.; Abed, J. A Navigation Strategy for Patient-Specific Needle Deflection in Transperineal MRI-Guided Prostate Interventions. *Brachytherapy* **2011**, *10*, S65. [CrossRef]
75. Scheer, J.K.; Hamelin, T.; Chang, L.; Lemkuil, B.; Carter, B.S.; Chen, C.C. Real-time Magnetic Resonance Imaging-Guided Biopsy Using SmartFrame® Stereotaxis in the Setting of a Conventional Diagnostic Magnetic Resonance Imaging Suite. *Oper. Neurosurg.* **2017**, *13*, 329–337. [CrossRef]
76. Wartenberg, M.; Schornak, J.; Carvalho, P.; Patel, N.; Iordachita, I.; Tempany, C.; Hata, N.; Tokuda, J.; Fischer, G.S. Closed-loop Autonomous Needle Steering during Cooperatively Controlled Needle Insertions for MRI-guided Pelvic Interventions. In *The Hamlyn Symposium*; Imperial College: London, UK, 2017. [CrossRef]
77. Wartenberg, M.; Patel, N.; Li, G.; Gregory, S.; Fischer, G.S. Towards synergistic control of hands-on needle insertion with automated needle steering for MRI-guided prostate interventions. In Proceedings of the 2016 38th Annual International Conference of the IEEE Engineering in Medicine and Biology Society (EMBC), Orlando, FL, USA, 16–20 August 2016; IEEE: Piscataway, NJ, USA, 2016. [CrossRef]
78. Wu, D.; Li, G.; Patel, N.; Yan, J.; Hu Kim, G.; Monfaredi, R.; Cleary, K.; Iordachita, I. Remotely Actuated Needle Driving Device for MRI-Guided Percutaneous Interventions: Force and Accuracy Evaluation. In Proceedings of the 2019 41st Annual International Conference of the IEEE Engineering in Medicine & Biology Society (EMBC), Berlin, Germany, 23–27 July 2019; IEEE: Piscataway, NJ, USA, 2019. [CrossRef]
79. Pons-Faudoa, F.P.; Ballerini, A.; Sakamoto, J.; Grattoni, A. Advanced implantable drug delivery technologies: Transforming the clinical landscape of therapeutics for chronic diseases. *Biomed. Microdevices* **2019**, *21*, 47. [CrossRef]
80. Minko, T. Drug delivery systems. In *Martin's Physical Pharmacy and Pharmaceutical Sciences*; Sinko, P.J., Ed.; Lippincott, Williams & Wilkins: Baltimore, MD, USA, 2006; pp. 629–680.
81. Stewart, S.A.; Dominguez-Robles, J.; Donnelly, R.F.; Larraneta, E. Implantable polymeric drug delivery devices: Classification, manufacture, materials, and clinical applications. *Polymers* **2018**, *10*, 1379. [CrossRef] [PubMed]
82. Santos, A.; Sinn, A.W.M.; Bariana, M.; Kumeria, T.; Wang, Y.; Losic, D. Drug-releasing implants: Current progress, challenges and perspectives. *J. Mater. Chem. B* **2014**, *2*, 6157–6182. [CrossRef] [PubMed]
83. Park, K. Controlled drug delivery systems: Past forward and future back. *J. Control. Release* **2014**, *190*, 3–8. [CrossRef] [PubMed]
84. Li, C.; Wang, J.; Wang, Y.; Gao, H.; Wei, G.; Huang, Y.; Yu, H.; Gan, Y.; Wang, Y.; Mei, L.; et al. Recent progress in drug delivery. *Acta Pharm. Sin. B* **2019**, *9*, 1145–1162. [CrossRef] [PubMed]
85. Kleiner, L.W.; Wright, J.C.; Wang, Y. Evolution of implantable and insertable drug delivery systems. *J. Control. Release* **2014**, *181*, 1–10. [CrossRef] [PubMed]
86. Yang, W.W.; Pierstorff, E. Reservoir-based polymer drug delivery systems. *J. Lab. Autom.* **2012**, *17*, 50–58. [CrossRef] [PubMed]

87. Kumar, A.; Pillai, J. Implantable drug delivery systems: An overview. In *Nanostructures for the Engineering of Cells, Tissues and Organs*; Grumezescu, A.M., Ed.; William Andrew Applied Science Publishers: Oxford, UK, 2018; pp. 473–511. [CrossRef]
88. Damiati, S.; Kompella, U.B.; Damiati, S.A.; Kodzius, R. Microfluidic Devices for Drug Delivery Systems and Drug Screening. *Genes* **2018**, *9*, 103. [CrossRef]
89. Davoodi, P.; Lee, L.Y.; Xu, Q.; Sunil, V.; Sun, Y.; Soh, S.; Wang, C.H. Drug delivery systems for programmed and on-demand release. *Adv. Drug Deliv. Rev.* **2018**, *132*, 104–138. [CrossRef]
90. Lee, H.J.; Choi, N.; Yoon, E.S.; Cho, I.J. MEMS devices for drug delivery. *Adv. Drug Deliv. Rev.* **2018**, *128*, 132–147. [CrossRef]
91. Beg, S.; Rahman, M.; Jain, A.; Saini, S.; Hasnain, M.S.; Swain, S.; Imam, S.; Kazmi, I.; Akhter, S. Emergence in the functionalized carbon nanotubes as smart nanocarriers for drug delivery applications. In *Fullerens, Graphenes and Nanotubes*; Elsevier: Amsterdam, The Netherlands, 2018; pp. 105–133. [CrossRef]
92. Antonino, R.S.C.M.Q.; Ruggiero, M.; Song, Z.; Nascimento, T.H.; Lima, E.M.; Bohr, A.; Knopp, M.M.; Löbmann, K. Impact of drug loading in mesoporous silica-amorphous formulations on the physical stability of drugs with high recrystallization tendency. *Int. J. Pharm. X* **2019**, *1*, 100026. [CrossRef]
93. Yang, P.M.; Mu, H.Z.; Zhang, Y.S.; Wang, W.C.; Liu, C.; Zhang, S.Y. Sequential release of immunomodulatory cytokines binding on nano-hydroxyapatite coated titanium surface for regulating macrophage polarization and bone regeneration. *Med. Hypotheses* **2020**, *144*, 110241. [CrossRef] [PubMed]
94. Häner, J.D.; Räber, L.; Windecker, S. Biodegradable vs. permanent polymer drug-eluting stents: The need for a new nomenclature to classify drug-eluting stent technology. *Eur. Heart J.* **2019**, *40*, 2616–2619. [CrossRef] [PubMed]
95. Razek, A. Towards an image-guided restricted drug release in friendly implanted therapeutics. *Eur. Phys. J. Appl. Phys.* **2018**, *82*, 31401. [CrossRef]
96. Razek, A. Assessment of Supervised Drug Release in Cordial Embedded Therapeutics. *Athens J. Technol. Eng.* **2019**, *6*, 77–91. [CrossRef]
97. Razek, A. Thermal effects of electromagnetic origin from heating processes to biological disturbances due to field exposure—A review. *Therm. Sci. Eng.* **2023**, *6*, 20–33. [CrossRef]
98. Cirimele, V.; Freschi, F.; Giaccone, L.; Pichon, L.; Repetto, M. Human Exposure Assessment in Dynamic Inductive Power Transfer for Automotive Applications. *IEEE Trans. Magn.* **2017**, *53*, 5000304. [CrossRef]
99. International Commission on Non-Ionizing Radiation Protection. Guidelines for limiting exposure to time-varying electric and magnetic fields for low frequencies (1 Hz–100 kHz). *Health Phys.* **2010**, *99*, 818–836. [CrossRef] [PubMed]
100. International Commission on Non-Ionizing Radiation Protection. Guidelines for limiting exposure to electromagnetic fields (100 kHz to 300 GHz). *Health Phys.* **2020**, *118*, 483–524. [CrossRef]
101. Den Boer, J.A.; Bourland, J.D.; Nyenhuis, J.A.; Ham, C.L.; Engels, J.M.; Hebrank, F.X.; Frese, G.; Schaefer, D.J. Comparison of the threshold for peripheral nerve stimulation during gradient switching in whole body MR systems. *J. Magn. Reason. Imaging* **2002**, *15*, 520–525. [CrossRef]
102. Mohith, S.; Upadhya, A.R.; Navin, K.P.; Kulkarni, S.M.; Rao, M. Recent trends in piezoelectric actuators for precision motion and their applications: A review. *Smart Mater. Struct.* **2020**, *30*, 013002. [CrossRef]
103. Gao, X.; Yang, J.; Wu, J.; Xin, X.; Li, Z.; Yuan, X.; Shen, X.; Dong, S. Piezoelectric Actuators and Motors: Materials, Designs, and Applications. *Adv. Mater. Technol.* **2020**, *5*, 1900716. [CrossRef]
104. Qiao, G.; Li, H.; Lu, X.; Wen, J.; Cheng, T. Piezoelectric stick-slip actuators with flexure hinge mechanisms: A review. *J. Intell. Mater. Syst. Struct.* **2022**, *33*, 1879–1901. [CrossRef]
105. Liu, J.; Gao, X.; Jin, H.; Ren, K.; Guo, J.; Qiao, L.; Qiu, C.; Chen, W.; He, Y.; Dong, S.; et al. Miniaturized electromechanical devices with multi-vibration modes achieved by orderly stacked structure with piezoelectric strain units. *Nat. Commun.* **2022**, *13*, 6567. [CrossRef] [PubMed]
106. Fu, D.K.; Fan, P.Q.; Yuan, T.; Wang, Y.S. A novel hybrid mode linear ultrasonic motor with double driving feet. *Rev. Sci. Instrum.* **2022**, *93*, 025003. [CrossRef] [PubMed]
107. Li, Z.; Guo, Z.; Han, H.; Su, Z.; Sun, H. Design and characteristic analysis of multi-degree-of-freedom ultrasonic motor based on spherical stator. *Rev. Sci. Instrum.* **2022**, *93*, 025004. [CrossRef] [PubMed]
108. Wang, S.; Zhou, S.; Zhang, X.; Xu, P.; Zhang, Z.; Ren, L. Bionic Stepping Motors Driven by Piezoelectric Materials. *J. Bionic Eng.* **2023**, *20*, 858–872. [CrossRef]
109. Hernandez, C.; Bernard, Y.; Razek, A. Design and manufacturing of a piezoelectric traveling-wave pumping device. *IEEE Trans. Ultrason. Ferroelectr. Freq. Control* **2013**, *60*, 1949–1956. [CrossRef]
110. Zhang, S.J.; Liu, Y.; Deng, J.; Gao, X.; Li, J.; Wang, W.Y.; Xun, M.X.; Ma, X.F.; Chang, Q.B.; Liu, J.K.; et al. Piezo robotic hand for motion manipulation from micro to macro. *Nat. Commun.* **2023**, *14*, 500. [CrossRef]
111. Yang, Z.; Li, X.; Tang, J.; Huang, H.; Zhao, H.; Cheng, Y.; Liu, S.; Li, C.; Xiong, M. A Bionic Stick–Slip Piezo-Driven Positioning Platform Designed by Imitating the Structure and Movement of the Crab. *J. Bionic Eng.* **2023**, *20*, 2590–2600. [CrossRef]
112. Virtanen, J. Enhancing the Compatibility of Surgical Robots with Magnetic Resonance Imaging. Ph.D. Thesis, University of Oulu, Oulu, Finland, 2006. Available online: http://urn.fi/urn:isbn:9514280660 (accessed on 1 November 2023).
113. Chinzei, K.; Kikinis, R.; Jolesz, F.A. MR compatibility of mechatronic devices: Design criteria. In Proceedings of the Medical Image Computing and Computer-Assisted Intervention—MICCAI'99, Cambridge, UK, 19–22 September 1999; Volume 1679, pp. 1020–1030. [CrossRef]

114. Chinzei, K.; Hata, N.; Jolesz, F.A.; Kikinis, R. Surgical assist robot for the active navigation in the intraoperative MRI: Hardware design issues. In Proceedings of the 2000 IEEE/RSJ International Conference on Intelligent Robots and Systems (IROS 2000) (Cat. No.00CH37113), Takamatsu, Japan, 31 October–5 November 2000; Volume 1, pp. 727–732. [CrossRef]
115. Tsekos, N.V.; Khanicheh, A.; Christoforou, E.; Mavroidis, C. Magnetic resonance-compatible robotic and mechatronics systems for image guided interventions and rehabilitation: A Review Study. *Annu. Rev. Biomed. Eng.* **2007**, *9*, 351–387. [CrossRef]
116. Tada, M.; Sasaki, S.; Ogasawara, T. Development of an optical 2-axis force sensor usable in MRI environments. In Proceedings of the SENSORS, 2002, Orlando, FL, USA, 12–14 June 2002; Volume 2, pp. 984–989. [CrossRef]
117. Tada, M.; Kanade, T. An MR-Compatible Optical Force Sensor for Human Function Modeling. In *Medical Image Computing and Computer-Assisted Intervention—MICCAI 2004*; Barillot, C., Haynor, D.R., Hellier, P., Eds.; Lecture Notes in Computer Science, 3217; Springer: Berlin/Heidelberg, Germany, 2004. [CrossRef]
118. Sedaghat, F.; Tuncali, K. Enabling Technology for MRI-Guided Intervention. *Top Magn. Reason. Imaging* **2018**, *27*, 5–8. [CrossRef] [PubMed]
119. Jolesz, F.A.; Morrison, P.R.; Koran, S.J.; Kelley, R.J.; Hushek, S.G.; Newman, R.W.; Fried, M.P.; Melzer, A.; Seibel, R.M.; Jalahej, H. Compatible instrumentation for intraoperative MRI: Expanding resources. *J. Magn. Reason. Imaging* **1998**, *8*, 8–11. [CrossRef] [PubMed]
120. Shellock, F.G. *Pocket Guide to MR Procedures and Metallic Objects: Update 1998*; Lippincott-Raven Publishers: Philadelphia, PA, USA, 1998. Available online: https://archive.org/details/pocketguidetomrp0000shel_y5n3 (accessed on 1 November 2023).
121. Schenck, J.F. The role of magnetic susceptibility in magnetic resonance imaging: MRI magnetic compatibility of the first and second kinds. *Med. Phys.* **1996**, *23*, 815–850. [CrossRef] [PubMed]
122. Razek, A. Assessment of EMF Troubles of Biological and Instrumental Medical Questions and Analysis of Their Compliance with Standards. *Standards* **2023**, *3*, 227–239. [CrossRef]
123. Razek, A. Assessment and Categorization of Biological Effects and Atypical Symptoms Owing to Exposure to RF Fields from Wireless Energy Devices. *Appl. Sci.* **2023**, *13*, 1265. [CrossRef]
124. Khairi, R.; Razek, A.; Bernard, L.; Corcolle, R.; Bernard, Y.; Pichon, L.; Poirier-Quinot, M.; Ginefri, J.C. EMC analysis of MRI environment in view of Optimized performance and cost of image guided interventions. *Int. J. Appl. Electromag. Mech.* **2016**, *51*, S67–S74. [CrossRef]
125. Nunes, A.S.; Dular, P.; Chadebec, O.; Kuo-Peng, P. Subproblems Applied to a 3-D Magnetostatic Facet FEM Formulation. *IEEE Trans. Magn.* **2018**, *54*, 7402209. [CrossRef]
126. Batra, T.; Schaltz, E.; Ahn, S. Effect of ferrite addition above the base ferrite on the coupling factor of wireless power transfer for vehicle applications. *J. Appl. Phys.* **2015**, *117*, 17D517. [CrossRef]
127. Piriou, F.; Razek, A. Numerical simulation of a nonconventional alternator connected to a rectifier. *IEEE Trans. Energy Convers.* **1990**, *5*, 512–518. [CrossRef]
128. Padilha, J.B.; Kuo-Peng, P.; Sadowski, N.; Batistela, N.J. Vector Hysteresis Model Associated to FEM in a Hysteresis Motor 691 Modeling. *IEEE Trans. Magn.* **2017**, *53*, 7402004. [CrossRef]
129. Ren, Z.; Razek, A. A coupled electromagnetic-mechanical model for thin conductive plate deflection analysis. *IEEE Trans. Magn.* **1990**, *26*, 1650–1652. [CrossRef]
130. Hariri, H.; Bernard, Y. Razek, 2-D Traveling Wave Driven Piezoelectric Plate Robot for Planar Motion. *IEEE ASME Trans. Mechatron.* **2018**, *23*, 242–251. [CrossRef]
131. Li, C.; Ren, Z.; Razek, A. An approach to adaptive mesh refinement for three-dimensional eddy-current computations. *IEEE Trans. Magn.* **1994**, *30*, 113–117. [CrossRef]
132. Grieves, M.; Vickers, J. Digital Twin: Mitigating Unpredictable, Undesirable Emergent Behavior in Complex Systems. In *Transdisciplinary Perspectives on Complex Systems*; Springer: Cham, Switzerland, 2017. [CrossRef]
133. Tao, F.; Sui, F.; Liu, A.; Qi, Q.; Zhang, M.; Song, B.; Guo, Z.; Lu, S.; Nee, A. Digital twin-driven product design framework. *Int. J. Prod. Res.* **2019**, *57*, 3935–3953. [CrossRef]
134. He, B.; Bai, K. Digital twin-based sustainable intelligent manufacturing: A review. *Adv. Manuf.* **2020**, *9*, 1–21. [CrossRef]
135. Rassõlkin, A.; Rjabtšikov, V.; Kuts, V.; Vaimann, T.; Kallaste, A.; Asad, B.; Partyshev, A. Interface Development for Digital Twin of an Electric Motor Based on Empirical Performance Model. *IEEE Access* **2022**, *10*, 15635–15643. [CrossRef]
136. Sun, T.; He, X.; Li, Z. Digital twin in healthcare: Recent updates and challenges. *Digit. Health* **2023**, *9*, 20552076221149651. [CrossRef]
137. Sun, T.; He, X.; Song, X.; Shu, L.; Li, Z. The Digital Twin in Medicine: A Key to the Future of Healthcare? *Front. Med.* **2022**, *9*, 907066. [CrossRef]
138. De Benedictis, A.; Mazzocca, N.; Somma, A.; Strigaroet, C. Digital twins in healthcare: An architectural proposal and its application in a social distancing case study. *IEEE J. Biomed. Health Inform.* **2022**, *27*, 5143–5154. [CrossRef]
139. Haleem, A.; Javaid, M.; Singh, R.P.; Suman, R. Exploring the revolution in healthcare systems through the applications of digital twin technology. *Biomed. Technol.* **2023**, *4*, 28–38. [CrossRef]
140. Mohamed, N.; Al-Jaroodi, J.; Jawhar, I.; Kesserwan, N. Leveraging Digital Twins for Healthcare Systems Engineering. *IEEE Access* **2023**, *11*, 69841–69853. [CrossRef]

141. Mohamed, N.; Al-Jaroodi, J.; Jawhar, I.; Kesserwan, N. How Healthcare Systems Engineering Can Benefit from Digital Twins? In Proceedings of the 2023 IEEE International Systems Conference (SysCon), Vancouver, BC, Canada, 17–20 April 2023; pp. 1–6. [CrossRef]
142. Ricci, A.; Croatti, A.; Montagna, S. Pervasive and Connected Digital Twins—A Vision for Digital Health. *IEEE Internet Comput.* **2022**, *26*, 26–32. [CrossRef]
143. Okegbile, S.D.; Cai, J. Edge-assisted human-to-virtual twin connectivity scheme for human digital twin frameworks. In Proceedings of the 2022 IEEE 95th Vehicular Technology Conference: (VTC2022-Spring), Helsinki, Finland, 19–22 June 2022; pp. 1–6. [CrossRef]
144. Das, C.; Mumu, A.A.; Ali, M.F.; Sarker, S.; Muyeen, S.; Kumar Das, S.; Das, P.; Hasan, M.M.; Tasneem, Z.; Islam, M.M.; et al. Toward IoRT Collaborative Digital Twin Technology Enabled Future Surgical Sector: Technical Innovations, Opportunities and Challenges. *IEEE Access* **2022**, *10*, 129079–129104. [CrossRef]
145. Moodley, D.; Seebregts, C. Re-imagining health and well-being in low resource African settings using an augmented AI system and a 3D digital twin. *arXiv* **2023**, arXiv:2306.01772. [CrossRef]
146. Strobel, G.; Möller, F.; van der Valk, H. Healthcare in the Era of Digital Twins: Towards a Domain-Specific Taxonomy. Tech. Rep. Healthcare IT, European Conference on Information Systems. 2022. Available online: https://api.semanticscholar.org/CorpusID:251034187 (accessed on 1 November 2023).
147. Song, Y. Human digital twin, the development and impact on design. *J. Comput. Inf. Sci. Eng.* **2023**, *23*, 060819. [CrossRef]
148. Burattini, S.; Montagna, S.; Croatti, A.; Gentili, N.; Ricci, A.; Leonardi, A.; Pandolfini, S.; Tosi, S. An Ecosystem of Digital Twins for Operating Room Management. In Proceedings of the 2023 IEEE 36th International Symposium on Computer-Based Medical Systems (CBMS), L'Aquila, Italy, 22–24 June 2023; pp. 770–775. [CrossRef]
149. Hagmann, K.; Hellings-Kuß, A.; Klodmann, J.; Richter, R.; Stulp, F.; Leidner, D. A Digital Twin Approach for Contextual Assistance for Surgeons During Surgical Robotics Training. *Front. Robot AI* **2021**, *8*, 735566. [CrossRef]
150. Gabriel, C.; Gabriel, S.; Corthout, E. The Dielectric Properties of Biological Tissues: II. Measurements in the Frequency Range 10 Hz to 20 GHz. *Phys. Med. Biol.* **1996**, *41*, 2251–2269. [CrossRef]
151. Barchanski, A.; Steiner, T.; De Gersem, H.; Clemens, M.; Weiland, T. Local Grid Refinement for low-Frequency Current Computations in 3-D Human Anatomy Models. *IEEE Trans. Magn.* **2006**, *42*, 1371–1374. [CrossRef]
152. Noetscher, G.M. The CAD-Compatible VHP-Male Computational Phantom. In *Brain and Human Body Modeling 2020: Computational Human Models Presented at EMBC 2019 and the BRAIN Initiative®2019 Meeting*; Makarov, S.N., Noetscher, G.M., Nummenmaa, A., Eds.; Springer: Cham, Switzerland, 2020; pp. 309–323. [CrossRef]
153. Makarov, S.N.; Noetscher, G.M.; Yanamadala, J.; Piazza, M.W.; Louie, S.; Prokop, A.; Nazarian, A.; Nummenmaa, A. Virtual Human Models for Electromagnetic Studies and Their Applications. *IEEE Rev. Biomed. Eng.* **2017**, *10*, 95–121. [CrossRef]
154. Shimron, E.; Perlman, O. AI in MRI: Computational Frameworks for a Faster, Optimized, and Automated Imaging Workflow. *Bioengineering* **2023**, *10*, 492. [CrossRef]
155. Seetohul, J.; Shafiee, M.; Sirlantzis, K. Augmented Reality (AR) for Surgical Robotic and Autonomous Systems: State of the Art, Challenges, and Solutions. *Sensors* **2023**, *23*, 6202. [CrossRef] [PubMed]
156. Avrumova, F.; Lebl, D.R. Augmented reality for minimally invasive spinal surgery. *Front. Surg.* **2023**, *9*, 1086988. [CrossRef] [PubMed]
157. Long, Y.; Cao, J.; Deguet, A.; Taylor, R.H.; Dou, Q. Integrating Artificial Intelligence and Augmented Reality in Robotic Surgery: An Initial dVRK Study Using a Surgical Education Scenario. In Proceedings of the 2022 International Symposium on Medical Robotics (ISMR), Atlanta, GA, USA, 13–15 April 2022; pp. 1–8. [CrossRef]
158. Fu, J.; Rota, A.; Li, S.; Zhao, J.; Liu, Q.; Iovene, E.; Ferrigno, G.; De Momi, E. Recent Advancements in Augmented Reality for Robotic Applications: A Survey. *Actuators* **2023**, *12*, 323. [CrossRef]
159. Qian, L.; Wu, J.Y.; DiMaio, S.P.; Navab, N.; Kazanzides, P. A Review of Augmented Reality in Robotic-Assisted Surgery. *IEEE Trans. Med. Robot. Bionics* **2020**, *2*, 1–16. [CrossRef]